Author/s:
Cooper, CM;Farrington, RJ;Miller, MS

Title:
On the Destructive Tendencies of Cratons

Date:
2020-10-07

Citation:
Cooper, C. M., Farrington, R. J. & Miller, M. S. (2020). On the Destructive Tendencies of Cratons. Geology, 49 (2), pp.195-200. https://doi.org/10.1130/G48111.1.

Persistent Link:
https://hdl.handle.net/11343/345556

GEOLOGY | THE GEOLOGICAL SOCIETY OF AMERICA®

https://doi.org/10.1130/G48111.1

Manuscript received 22 February 2020
Revised manuscript received 7 July 2020
Manuscript accepted 27 August 2020

Published online XX Month 2020

On the destructive tendencies of cratons

C.M. Cooper[1]*, R.J. Farrington[2] and M.S. Miller[3]
[1]School of the Environment, Washington State University, Pullman, Washington 99164, USA
[2]School of Earth Sciences, The University of Melbourne, Melbourne, Victoria 3010, Australia
[3]Research School of Earth Sciences, The Australian National University, Canberra, Australian Capital Territory 2600, Australia

ABSTRACT

We propose that subducting slabs may cause lithospheric removal by directing mantle flow along the craton margin. This process could carve and shape the cratons, leading to conditions that impact the overall (in)stability of the lithosphere. We use three-dimensional geodynamic models to investigate how subduction-driven directed flow interacts with cratonic lithosphere of differing shape, concluding that the margin shape controls both channelization of flow around the craton as well as the potential for destruction. While the simulations show that all craton shapes aid in channelization, the cratons with straight vertical margins are the most resistant to deformation, and the cratons with gradually thickening margins are less resistant to deformation. The dependence on shape could contribute to the progressive removal of cratonic lithosphere along its margin in a runaway process until a more stable vertical margin shape evolves.

INTRODUCTION

Subducting slabs drive large-scale flow patterns in the uppermost mantle that are, at times, directed along the margins of cratons, creating the potential for destruction of seemingly indestructible lithosphere. For example, the tectonic setting of the northern margin of both South America and northwestern Africa place subducting slabs near cratonic lithosphere (Fig. 1A). In these regions, mantle flow has been inferred from joint interpretation of seismic anisotropy observations and geodynamic modeling (Miller and Becker, 2012; Alpert et al., 2013) to be directed by the subducted slabs toward the cratons. Seismic anisotropy inferred from shear-wave splitting can be used as a constraint on first-order patterns of mantle convection and deformational processes within the Earth. Strain aligns highly anisotropic minerals (e.g., olivine) in the mantle, which is the primary source of seismic anisotropy in the mantle (Long and Becker, 2010). Shear-wave splitting results (Russo and Silver, 1994; Russo et al., 1996; Growdon et al., 2009; Masy et al., 2011) for northern South America have anomalously large delay times and are oriented parallel to the east-west–striking plate boundary with the Caribbean plate (Fig. 1B). These have been interpreted as resulting from strong vertical shear due to eastward mantle flow coupled with the motion of the subducted slab, which decreases in magnitude southward toward the thickest regions of the Amazonian craton (Miller and Becker, 2012). In northwestern Africa (Fig. 1C), shear-wave splitting results (Diaz et al., 2010; Miller et al., 2013; Díaz and Gallart, 2014) illustrate complex patterns of mantle flow due to the slab descending beneath the Gibraltar arc and the position of the West African craton. Small-amplitude delay times are found at stations within the craton, while large-amplitude, similarly aligned splitting measurements are present at stations in the Atlas Mountains (Morocco) on the thinnest continental lithosphere (Miller et al., 2013, 2015; Miller and Becker, 2014). In both settings, it has been suggested that mantle flow is channelized due to the geometry of the subducted slabs and the cratonic lithosphere (Miller and Becker, 2012, 2014; Alpert et al., 2013).

The craton margins in both settings demonstrate progressive lithospheric thickening toward the interior of the craton (see the Supplemental Material[1] for the full geometry description). The northern Amazonian craton thickness increases through a series of tiers of increasing thickness (Heintz et al., 2005; Feng et al., 2007; Miller et al., 2009; Pasyanos et al., 2014; Masy et al., 2015), whereas the northwestern margin of the West African craton gently increases in thickness, following a diagonal shape (Fishwick, 2010; Pasyanos et al., 2014; Miller et al., 2015) (Fig. 1). Seismic images demonstrate that there is a wide range of craton margin shapes, including those mentioned above and ranging to sharp, vertical edges stepping from average continental thickness to thick cratonic cores (e.g., Fishwick et al., 2008; Bao et al., 2014; Foster et al., 2014; Miller et al., 2015; Chen et al., 2019). These craton margin shapes likely influence channelization of mantle flow, but could also be indicative of the current and past status of the craton. The controls on craton margin shape are not clear, but Currie and van Wijk (2016) demonstrated that a range of craton shapes can be maintained over time scales of >100 m.y. or can be deformed into other shapes depending on the rheology and composition of the modeled cratonic lithosphere.

Understanding how cratons are affected by the flow induced by subducting slabs provides additional insight into their stability. Can directed flow erode, thin, and shape the craton along its edges? How much does the shape of cratons control deformation and/or mantle flow? We address these questions using geodynamic models to investigate the potential for directed mantle flow to erode craton margins and whether this flow is dependent on the shape of the craton.

METHOD AND RESULTS

Channelized Flow and Increased Potential for Deformation

Using the geodynamic code Underworld (Moresi et al., 2007, 2018; https://www.underworldcode.org/tag/underworld-code/), we modeled the instantaneous flow field and deformation of a mantle, craton, and slab system for different margin shapes (Fig. 2;

*E-mail: cmcooper@wsu.edu

[1]Supplemental Material. Detailed methodology of models and post-processing. Please visit https://doi.org/10.1130/XXXXX to access the supplemental material, and contact editing@geosociety.org with any questions.

CITATION: Cooper, C.M., Farrington, R.J., and Miller, M.S., 2020, On the destructive tendencies of cratons: Geology, v. 49, p. XXX–XXX, https://doi.org/10.1130/G48111.1

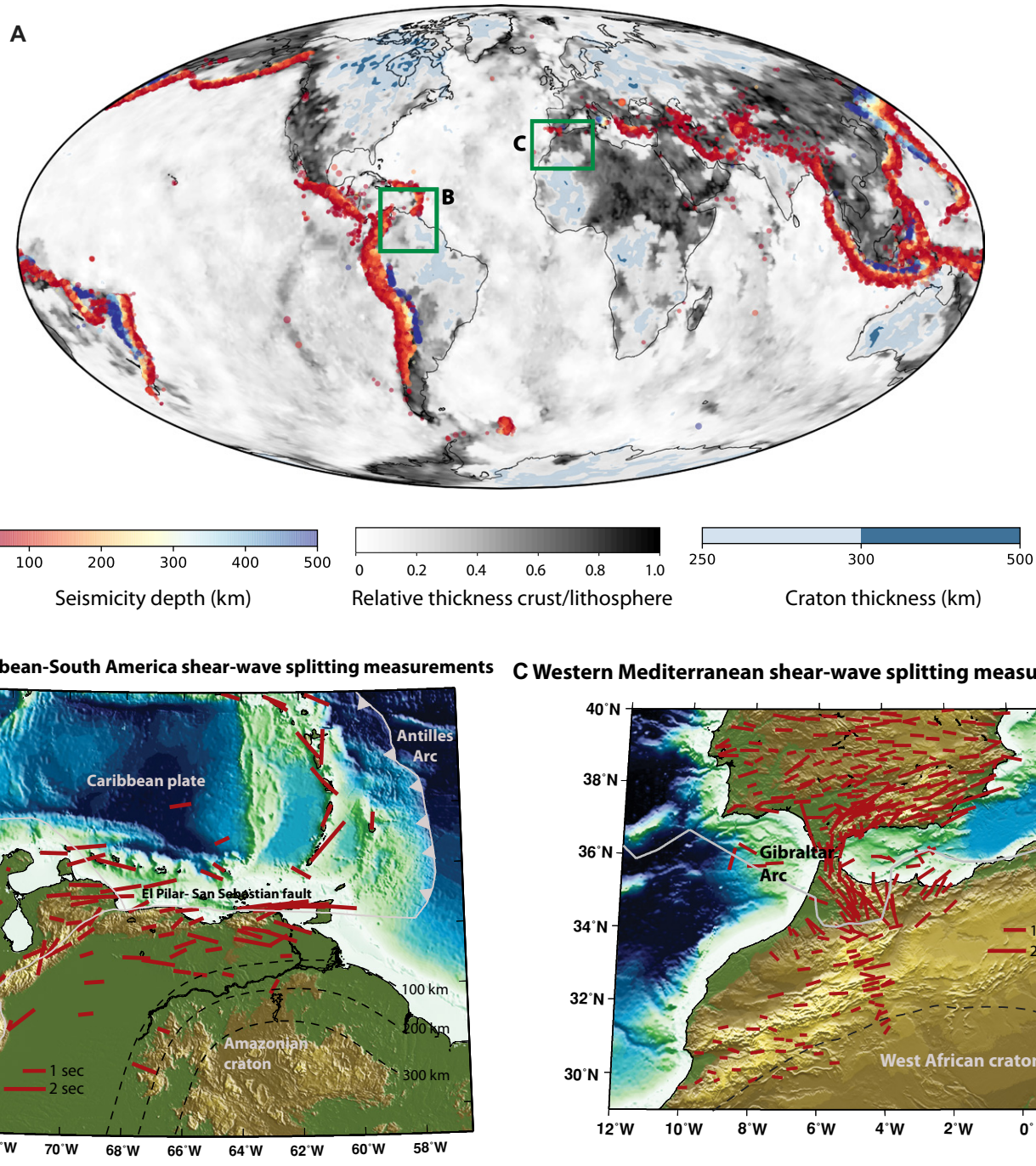

Figure 1. (A) Global map illustrating locations of subduction zones with Wadati-Benioff zone seismicity M >4.5 (>50 km depth) illustrating dip of slabs and locations of cratons and their variable margin shapes. Cratons are shown in blue colors (note craton color scale increments), as represented by lithospheric thickness estimates from LITHO1.0 model (Pasyanos et al., 2014; https://igppweb.ucsd.edu/~gabi/litho1.0.html). Locations of B and C are shown with green rectangles. (B) Regional map of the Caribbean–South America plate boundary with shear-wave splitting measurements. Plate boundaries are plotted as gray lines (Bird, 2003). Black dotted lines are inferred position of the Amazonian craton (100 km steps) from Miller and Becker (2012). Average SK(K)S splitting is shown with red bars using the updated database from Becker et al. (2012). Background image is from ETOPO1 (https://doi.org/10.7289/V5C8276 M). (C) Regional map of the westernmost Mediterranean and northwestern Africa with shear-wave splitting measurements. Plate boundaries are plotted as gray lines (Bird, 2003). Black dotted line is inferred margin of the West African craton at ~200 km depth, from Miller et al. (2015). Average SK(K)S splitting is shown with red bars using the updated database from Becker et al. (2012). Small-amplitude delay times are found at stations within the craton, large-amplitude outside the craton, where splits then change amplitude and orientation into an arcuate-shape pattern indicating circum-slab flow to the north at the Gibraltar arc.

Figs. S1–S4 in the Supplemental Material). Our models explore the modification of the cratonic lithosphere due to its interaction with mantle flow induced by a slab positioned orthogonal to a continent (similar to tectonic settings in Figs. 1B and 1C). We considered three scenarios: craton-only models, subducting slab–only models, and models that included both the craton and the subducting slab (Table S2). Within the three scenarios, we chose four margin shapes—a vertical, straight margin directly adjacent to the subducting slab ("straight proximal"); a vertical, straight margin located 300 km to the south of the subducting slab ("straight distal"); a tiered margin, increasing in thickness southward in three steps (tiered); and a diagonal margin, progressively thickening southward (diagonal) (Fig. S1)—to encompass the range of margins

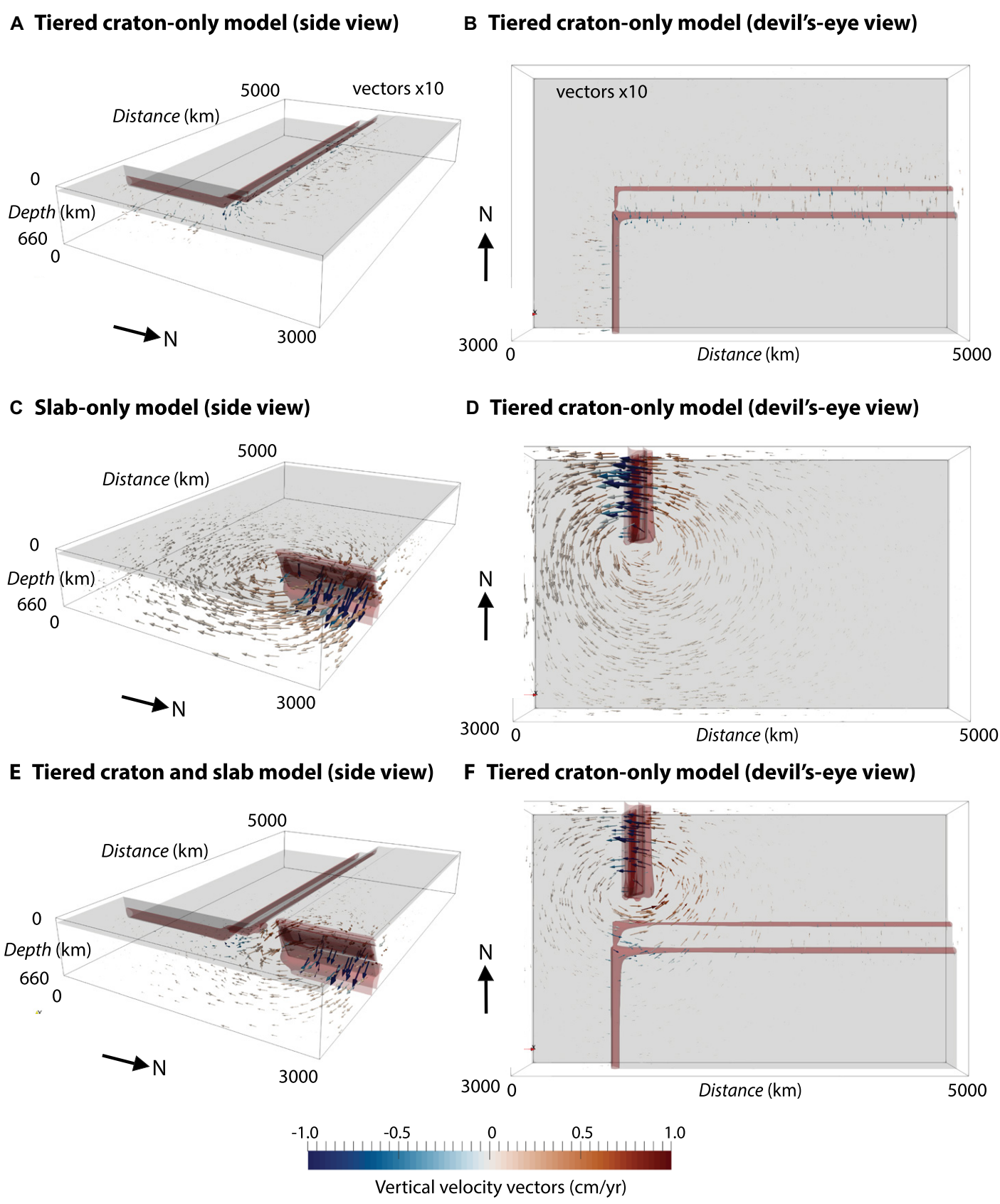

Figure 2. Mantle flow (vectors) with temperature (gray) and dissipation (red) contours for the tiered craton-only model (A,B), slab-only model (C,D), and tiered-craton and slab model (E,F). For visualization purposes, the length of vectors in A and B was scaled by 10× compared to those in C–F, highlighting the difference in magnitude between mantle flow driven by subduction and edge-driven convection. Panels on the right are "devil's-eye view" from the base of the model; panels on left are viewed from the northeast. We use "devil's-eye view" to better visualize flow along the complex craton margin that might be masked by looking from above. Temperature contour is at 1400 K; dissipation contour at 2 × 10^{-9} Pa/s. Velocity vectors are colored by vertical velocity, with maximum length scaled to 0.56 cm/yr for A and B and 5.6 cm/yr for C–F.

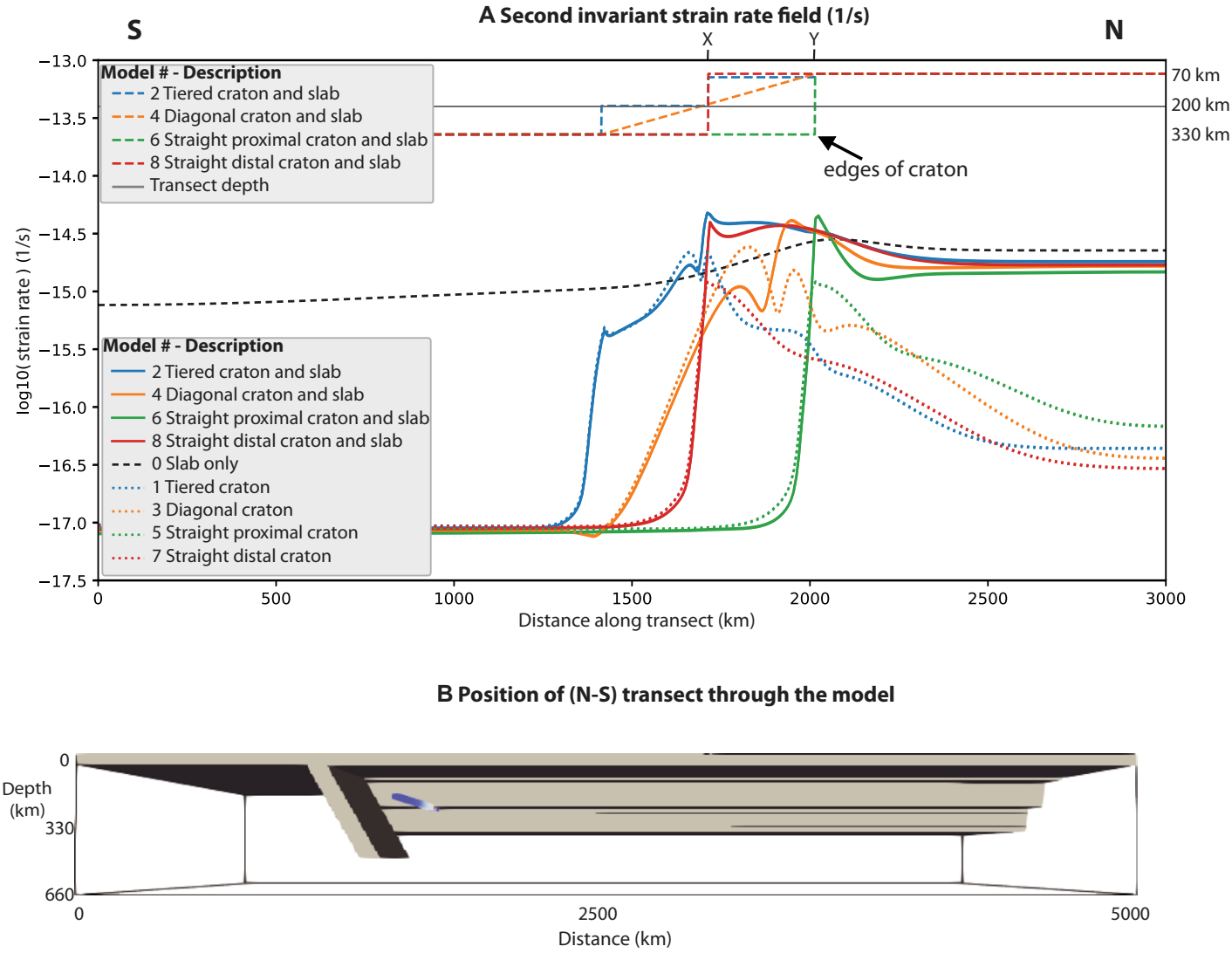

Figure 3. Strain-rate transects. (A) Second invariant of strain rate (1/s) along the north-south transect shown with blue tracers in B, sampled at a depth of 198 km and directly to the west of the subducting slab as viewed from the north. Transect (gray line) runs parallel to the strike of slab, and samples regions within the mantle wedge extending into the cratonic lithosphere. Solid lines show values for slab and craton models, while dotted lines show values for craton-only models. For reference, dashed lines show position and prescribed shape of the craton. Label X marks position of the edge of the craton for the straight-margin distal craton (models 7 and 8) as well as where the transect enters the diagonal-margin craton (models 3 and 4), and where the transect runs along the base of the tiered-margin craton (models 1 and 2). Label Y marks position of the edge of the craton for the straight-margin proximal craton (models 5 and 6). Transect intersects the deepest portion of the tiered margin craton at 1400 km. Model numbering follows Table S2 (see footnote 1). (B) View from the north showing location of the transect line (in blue) for the tiered-craton and slab model (Figs. 2E and 2F). Transect line is in the same location for all models.

observed for cratons (e.g., Bao et al., 2014; Masy et al., 2015; Miller et al., 2015).

We used a three-dimensional Cartesian model domain of length 5000 km (west-east), width 3000 km (north-south), and height 660 km. The craton region within the model spanned the southwestern region of the domain, having dimensions 4000 km (length) × 1400 km (width) × 330 km (depth, defined by the 1400 K isotherm) with a northern margin width of 600 km and variable depths depending on chosen margin geometry (Fig. S1). The slab, spanning 1000 km, representing subducted oceanic lithosphere with a thickness of 100 km and dipping 60° to the west to a depth of 495 km. The temperature fields are defined by inverting the half-space cooling model (Turcotte and Schubert, 2014) for the cratonic, oceanic plate, and subducting slab thickness at 1400 K, approximating the base of the lithosphere. We used temperature- and strain rate–dependent viscosity and free-slip velocity boundary conditions on all sides (see the Supplementary Material and Table S1 for model parameters).

Mantle flow in our models is driven by (1) the negative thermal buoyancy of the slab, and (2) the thermal boundary layer between craton and mantle. The subduction-induced mantle flow is produced by the negative thermal buoyancy as well the rigidity of the continuous surface plate and subducting slab. This combination simulates slab rollback that produces the largely horizontal mantle flow. Figure 2 illustrates the flow patterns produced in the models. Figures 2A and 2B show the flow field for a craton-only model with a tiered margin (see Figs. S3 and S4 for other margin shapes). The flow field in this scenario is dominated by small-scale (edge-driven) convection, driven by lateral temperature variations, within the thermal boundary layer between the craton and the mantle. Figures 2C and 2D show the flow field for a model with a slab only, highlighting the much larger-scale subduction-driven mantle flow. The velocity field is characterized by large-scale toroidal flow circulating from behind the slab around the mantle adjacent to the subducting plate and into the mantle wedge. The flow resulting from the

interaction of the craton and subducting slab is shown in Figures 2E and 2F. The interaction can be identified in three related processes: (1) large-scale dampening of the toroidal, slab-induced mantle flow by the presence of the craton, (2) the small-scale edge-driven convection produced by the lateral thermal discontinuities introduced by the craton, and (3) deflection and localization of the toroidal flow within the margin between the slab and craton.

Moving Deformation Inward

This channelization can lead to deformation of the cratonic lithosphere depending on the margin shape. Figure 3 shows north-south transects that sampled strain rate in the region directly to the west of the subducting slab at a depth of 197 km (transect location in Fig. 3C). These north-south transects sample the mantle wedge, the channel, and the cratonic lithosphere. The transect enters the cratonic lithosphere at different points depending on the margin geometry (top portion of Fig. 3A, intersection points labeled as "X" and "Y").

Channelized flow increased the strain rate of the mantle flow within the channel as well as within the cratonic lithosphere (Fig. 3A). The degree of this increase as well as how far the increased strain rate extended laterally into the craton depended on the margin shape (Fig. 3A). The increased strain rate extends farther laterally into the craton interior for the diagonal- and tiered-shape margins (solid orange and blue lines, respectively; the transect enters the craton or runs along its base at X). The increase in strain rate is dampened by several orders of magnitude when moving farther into the craton interior for both simulations of straight, vertical margins (at "X" for straight distal and "Y" for straight proximal) regardless of the location of the margin (relative to the slab) and channel size (solid green and red lines in Fig. 3A). This suggests that straight, vertical margins are a more stable shape compared to those with progressive thickening into the interior.

DISCUSSION

This dependence on margin shape follows the premise that craton stability is linked to lithospheric thickness (Lenardic and Moresi, 1999; Cooper et al., 2006). The tiered and diagonal margins place thinner lithosphere in proximity to increased mantle flow, subjecting the craton to deformation. The straight, vertical margin, however, positions thick, cold, rheologically strong (as driven by the thermal structure) lithosphere near the enhanced flow. The thicker, and thus stronger, lithosphere suppresses the potential for deformation, as demonstrated by both straight-margin scenarios. When the slab is present, the increased mantle flow velocities are pushed toward the craton and result in an increase in strain rate directly along the margin. For thin margins, this can result in deformation contributing to further thinning of the cratonic lithosphere, which could lead to progressive erosion of the margin until a more stable shape evolved. Thus, as the simulations demonstrate, the result of a complex margin geometry, such as a tiered or diagonal shape, is twofold: the introduction of a channel to localize mantle flow, and the placement of thinner, weaker lithosphere along the margin, both of which increase the potential for destruction of the craton.

These results suggest two possible interpretations: (1) progressive deformation of cratonic margins may modify the shape from tiered or diagonal to a more stable straight, vertical margin, or (2) straight, vertical margins may be long-lived features remnant of either formation or catastrophic deformation. The first interpretation suggests that increased mantle flow can lead to craton destruction through runaway processes occurring along the margins moving toward the interior. This is different than previously proposed models for craton destruction that invoke large-scale events such as delamination of much or all of the lithosphere (e.g., Kay and Mahlburg Kay, 1993; Liu et al., 2018) or gravitational instabilities within the lower lithosphere (e.g., Hu et al., 2018). The second interpretation indicates that caution is needed when interpreting seismic images of straight, vertical cratonic margins. It may be tempting to suggest that the abrupt change in lithospheric thickness is evidence for a large, catastrophic event (Bao et al., 2014); however, it is possible that the shape is a remnant of the processes that formed the craton.

Note that our simulations assume a rheologically strong cratonic lithosphere consistent with observations of dehydrated cratonic xenoliths (Peslier et al., 2010). Currie and van Wijk (2016) demonstrated that weaker rheology leads to relaxation of a straight, vertical margin into a more diagonal shape while stronger rheology ensures preservation of the initially vertical shape. This suggests an interplay between margin shape and rheology, with some geometries possible only for certain rheological properties.

CONCLUSIONS

Directed mantle flow channelized along a craton can impact a craton's stability, depending on the shape of the craton margin. Straight, vertical margins dramatically dampen the enhanced flow, protecting the craton interior from deformation. Progressively thickening margins, however, allow for the increased strain rate to extend into the interior of the craton, increasing the potential for deformation. We note that this trend strikingly follows the observed shear wave patterns in South America and northwestern Africa as shown in Figures 1B and 1C. For these tectonic settings with non-vertical craton margins, the change in the shear-wave splitting amplitudes suggest an inward progression of deformation, with the largest delay times adjacent to the plate boundaries within the mantle channel. Rather than a rapid diminishing of amplitudes, the observed shear-wave splitting delay times progressively decrease southward into cratonic interiors. The large-amplitude splits aligned with the strike of the craton margin illustrate that the mantle flow and therefore inferred deformation of the continental lithosphere are constrained by the geometry of the craton. This suggests that in these regions, cratons could be progressively eroding along their nonvertical edges.

ACKNOWLEDGMENTS

Cooper was supported by the U.S. National Science Foundation (NSF) (grant EAR-1112820), Farrington was supported by the Australian Research Council (grant DP130101946), and Miller was supported by the NSF (grant EAR-1054638). This work used XSEDE (Extreme Science and Engineering Discovery Environment; https://www.xsede.org), which is supported by NSF grant number ACI-1548562. This work was enabled by Auscope (Melbourne, Australia) and the National Computational Infrastructure (NCI), which are supported by the Australian Government via the National Collaborative Research Infrastructure Strategy (NCRIS). We appreciate the constructive feedback from the reviewers of this paper.

REFERENCES CITED

Alpert, L.A., Miller, M.S., Becker, T.W., and Allam, A.A., 2013, Structure beneath the Alboran from geodynamic flow models and seismic anisotropy: Journal of Geophysical Research: Solid Earth, v. 118, p. 4265–4277, https://doi.org/10.1002/jgrb.50309.

Bao, X.W., Eaton, D.W., and Guest, B., 2014, Plateau uplift in western Canada caused by lithospheric delamination along a craton edge: Nature Geoscience, v. 7, p. 830–833, https://doi.org/10.1038/ngeo2270.

Becker, T.W., Lebedev, S., and Long, M.D., 2012, On the relationship between azimuthal anisotropy from shear wave splitting and surface wave tomography: Journal of Geophysical Research, v. 117, B01306, https://doi.org/10.1029/2011JB008705.

Bird, P., 2003, An updated digital model of plate boundaries: Geochemistry Geophysics Geosystems, v. 4, 1027, https://doi.org/10.1029/2001GC000252.

Chen, Y.F., Gu, Y.J., Currie, C.A., Johnston, S.T., Hung, S.H., Schaeffer, A.J., and Audet, P., 2019, Seismic evidence for a mantle suture and implications for the origin of the Canadian Cordillera: Nature Communications, v. 10, 2249, https://doi.org/10.1038/s41467-019-09804-8.

Cooper, C.M., Lenardic, A., Levander, A., and Moresi, L., 2006, Creation and preservation of cratonic lithosphere: Seismic constraints and geodynamic models, *in* Benn, K., et al., eds., Archean Geodynamics and Environments: American Geophysical Union Geophysical Monograph 164, p. 75–88, https://doi.org/10.1029/164GM07.

Currie, C.A., and van Wijk, J., 2016, How craton margins are preserved: Insights from geodynamic models: Journal of Geodynamics, v. 100, p. 144–158, https://doi.org/10.1016/j.jog.2016.03.015.

Díaz, J., and Gallart, J., 2014, Seismic anisotropy from the Variscan core of Iberia to the Western African Craton: New constraints on upper mantle flow at regional scales: Earth and Planetary Science Letters, v. 394, p. 48–57, https://doi.org/10.1016/j.epsl.2014.03.005.

Diaz, J., Gallart, J., Villaseñor, A., Mancilla, F., Pazos, A., Córdoba, D., Pulgar, J.A., Ibarra, P., and Harnafi, M., 2010, Mantle dynamics beneath the Gibraltar Arc (western Mediterranean) from shear-wave splitting measurements on a dense seismic array: Geophysical Research Letters, v. 37, L18304, https://doi.org/10.1029/2010GL044201.

Feng, M., van der Lee, S., and Assumpção, M., 2007, Upper mantle structure of South America from joint inversion of waveforms and fundamental mode group velocities of Rayleigh waves: Journal of Geophysical Research, v. 112, B04312, https://doi.org/10.1029/2006jb004449.

Fishwick, S., 2010, Surface wave tomography: Imaging of the lithosphere-asthenosphere boundary beneath central and southern Africa?: Lithos, v. 120, p. 63–73, https://doi.org/10.1016/j.lithos.2010.05.011.

Fishwick, S., Heintz, M., Kennett, B.L.N., Reading, A.M., and Yoshizawa, K., 2008, Steps in lithospheric thickness within eastern Australia: Evidence from surface wave tomography: Tectonics, v. 27, TC4009, https://doi.org/10.1029/2007TC002116.

Foster, K., Dueker, K., Schmandt, B., and Yuan, H., 2014, A sharp cratonic lithosphere-asthenosphere boundary beneath the American Midwest and its relation to mantle flow: Earth and Planetary Science Letters, v. 402, p. 82–89, https://doi.org/10.1016/j.epsl.2013.11.018.

Growdon, M.A., Pavlis, G.L., Niu, F.L., Vernon, F.L., and Rendon, H., 2009, Constraints on mantle flow at the Caribbean–South American plate boundary inferred from shear wave splitting: Journal of Geophysical Research, v. 114, B02303, https://doi.org/10.1029/2008JB005887.

Heintz, M., Debayle, E., and Vauchez, A., 2005, Upper mantle structure of the South American continent and neighboring oceans from surface wave tomography: Tectonophysics, v. 406, p. 115–139, https://doi.org/10.1016/j.tecto.2005.05.006.

Hu, J.S., Liu, L.J., Faccenda, M., Zhou, Q., Fischer, K.M., Marshak, S., and Lundstrom, C., 2018, Modification of the Western Gondwana craton by plume-lithosphere interaction: Nature Geoscience, v. 11, p. 203–210, https://doi.org/10.1038/s41561-018-0064-1.

Kay, R.W., and Mahlburg Kay, S., 1993, Delamination and delamination magmatism: Tectonophysics, v. 219, p. 177–189, https://doi.org/10.1016/0040-1951(93)90295-U.

Lenardic, A., and Moresi, L.-N., 1999, Some thoughts on the stability of cratonic lithosphere: Effects of buoyancy and viscosity: Journal of Geophysical Research, v. 104, p. 12,747–12,758, https://doi.org/10.1029/1999JB900035.

Liu, L., Morgan, J.P., Xu, Y.G., and Menzies, M., 2018, Craton destruction 1: Cratonic keel delamination along a weak midlithospheric discontinuity layer: Journal of Geophysical Research: Solid Earth, v. 123, p. 10,040–10,068, https://doi.org/10.1029/2017JB015372.

Long, M.D., and Becker, T.W., 2010, Mantle dynamics and seismic anisotropy: Earth and Planetary Science Letters, v. 297, p. 341–354, https://doi.org/10.1016/j.epsl.2010.06.036.

Masy, J., Niu, F.L., Levander, A., and Schmitz, M., 2011, Mantle flow beneath northwestern Venezuela: Seismic evidence for a deep origin of the Mérida Andes: Earth and Planetary Science Letters, v. 305, p. 396–404, https://doi.org/10.1016/j.epsl.2011.03.024.

Masy, J., Niu, F.L., Levander, A., and Schmitz, M., 2015, Lithospheric expression of Cenozoic subduction, Mesozoic rifting and the Precambrian Shield in Venezuela: Earth and Planetary Science Letters, v. 410, p. 12–24, https://doi.org/10.1016/j.epsl.2014.08.041.

Miller, M.S., and Becker, T.W., 2012, Mantle flow deflected by interactions between subducted slabs and cratonic keels: Nature Geoscience, v. 5, p. 726–730, https://doi.org/10.1038/ngeo1553.

Miller, M.S., and Becker, T.W., 2014, Reactivated lithospheric-scale discontinuities localize dynamic uplift of the Moroccan Atlas Mountains: Geology, v. 42, p. 35–38, https://doi.org/10.1130/G34959.1.

Miller, M.S., Levander, A., Niu, F.L., and Li, A., 2009, Upper mantle structure beneath the Caribbean–South American plate boundary from surface wave tomography: Journal of Geophysical Research, v. 114, B01312, https://doi.org/10.1029/2007JB005507.

Miller, M.S., Allam, A.A., Becker, T.W., Di Leo, J.F., and Wookey, J., 2013, Constraints on the tectonic evolution of the westernmost Mediterranean and northwestern Africa from shear wave splitting analysis: Earth and Planetary Science Letters, v. 375, p. 234–243, https://doi.org/10.1016/j.epsl.2013.05.036.

Miller, M.S., O'Driscoll, L.J., Butcher, A.J., and Thomas, C., 2015, Imaging Canary Island hotspot material beneath the lithosphere of Morocco and southern Spain: Earth and Planetary Science Letters, v. 431, p. 186–194, https://doi.org/10.1016/j.epsl.2015.09.026.

Moresi, L., Quenette, S., Lemiale, V., Mériaux, C., Appelbe, B., and Mühlhaus, H.-B., 2007, Computational approaches to studying non-linear dynamics of the crust and mantle: Physics of the Earth and Planetary Interiors, v. 163, p. 69–82, https://doi.org/10.1016/j.pepi.2007.06.009.

Moresi, L., et al., 2018, Underworld2: Python Geodynamics Modelling for Desktop, HPC and Cloud, Version 2: https://doi.org/10.5281/zenodo.1436039 (accessed October 2017).

Pasyanos, M.E., Masters, T.G., Laske, G., and Ma, Z.T., 2014, LITHO1.0: An updated crust and lithospheric model of the Earth: Journal of Geophysical Research: Solid Earth, v. 119, p. 2153–2173, https://doi.org/10.1002/2013JB010626.

Peslier, A.H., Woodland, A.B., Bell, D.R., and Lazarov, M., 2010, Olivine water contents in the continental lithosphere and the longevity of cratons: Nature, v. 467, p. 78–81, https://doi.org/10.1038/nature09317.

Russo, R.M., and Silver, P.G., 1994, Trench-parallel flow beneath the Nazca plate from seismic anisotropy: Science, v. 263, p. 1105–1111, https://doi.org/10.1126/science.263.5150.1105.

Russo, R.M., Silver, P.G., Franke, M., Ambeh, W.B., and James, D.E., 1996, Shear-wave splitting in northeast Venezuela, Trinidad, and the eastern Caribbean: Physics of the Earth and Planetary Interiors, v. 95, p. 251–275, https://doi.org/10.1016/0031-9201(95)03128-6.

Turcotte, D., and Schubert, G., 2014, Geodynamics (third edition): Cambridge, UK, Cambridge University Press, 623 p., https://doi.org/10.1017/CBO9780511843877.

Printed in USA